# The effect of intermediate nucleotide binding affinities on the rotation of $F_1-$ATPase: a brownian dynamics study

Camilo Aponte-Santamaría [1]
Simulation of Physical Systems Group, Department of Physics,
Universidad Nacional de Colombia, and CeiBA - Complejidad,
Bogotá, Colombia

J. Alfonso Leyva [2]
Department of Biophysics and Biophysical Chemistry
Johns Hopkins University School of Medicine, Baltimore, Maryland

José Daniel-Muñoz [3]
Simulation of Physical Systems Group, Department of Physics,
Universidad Nacional de Colombia, and CeiBA - Complejidad,
Bogotá, Colombia

[1]Present address: Computational Biomolecular Dynamics Group, Max Planck Institute for Biophysical Chemistry, Am Fassberg 11, 37077 Göttingen, Germany

[2]Present address: Department of Physics and Center for Biotechnology and Interdisciplinary Studies, Rensselaer Polytechnic Institute, 110 8ht Street Troy, NY 12180, USA.

[3]Corresponding author. Address: Simulation of Physical Systems Group, Department of Physics, Universidad Nacional de Colombia, and CeiBA - Complejidad, Avenida 30 No. 45-03, Edificio 404, Oficina 348, Bogotá, Colombia, Tel.: (571)316-5000, Ext. 13031, Fax: (571)316-5135

**Abstract**

$F_1-$ATPase is a molecular motor that is able to rotate huge artifacts, two orders of magnitude larger than the motor itself, such as actin filaments or gold beads. The sequence of catalytic events that this molecular machine follows during rotation has been fully established. Nevertheless, the conformation of the β subunits at each stage of the rotational cycle remains to be elucidated. Hereby, we investigate the effect of intermediate nucleotide binding affinities on the rotation of an actin filament when is propelled by the F1 motor, by using Brownian dynamics and a reduced set of kinetic equations. Two hydrolysis pathways were compared: a 3-State pathway, including three conformational states for the β subunits with nucleotide binding affinities "Open", "Loose" and "Tight", and a 4-State pathway, adding a fourth intermediate state "Closed", that could be paired with an ATP (ADP) binding affinity of $K_D$=30 $\mu$M (35 $\mu$M). Our simulations with the 4-State pathway reproduce extraordinary well the experimental frequencies for a wide range of ATP concentrations (20nM to 20mM) and filament lengths (0.5 $\mu$M to 4 $\mu$M). In contrast, the 3-State pathway gives frequencies that are systematically lower than observed, emphasizing therefore in the relevance of the intermediate "Closed" state.

*Key words:* Molecular motors; Energy transduction; ATP synthesis; Computer simulations

# 1 Introduction

ATP-Syntase is not only the manufacture center of ATP in mitochondria, chloroplasts and bacteria, but also the source of promising molecular motors of future nanotechnological applications. In a series of experiments (1, 2), it was shown by direct observations through an optical microscope that the $F_1-$ATPase alone, i. e. the soluble part of the ATP-Synthase, works as a rotary molecular motor, driven by the hydrolysis of ATP. This motor is able to propel huge organic and inorganic devices, even two orders of magnitude larger than the motor itself, such as actin filaments or gold beads (1–11), with an energy conversion efficiency near 100% (2, 6). From these experiments, it has been possible to establish that the rotation of the $\gamma$ subunit of the $F_1-$ATPase occurs at discrete steps of $120^\circ$, corroborating the *binding change* mechanism initially proposed by Boyer (12, 13). It has been also shown that each $120^\circ$ rotation is divided into four substeps (figure 1): an ATP-binding dwell time, with an ATP association constant of $\sim 2\times 10^7$ $M^{-1}s^{-1}$ from a range of ATP concentrations from nanomolar to milimolar (9); a $80^\circ$ rapid rotation, where $F_1$ excerts a constant torque closer to 40 pN·nm over the actin filament (for the same range of concentrations mentioned before) (7, 9); a catalytic dwell time of $\sim 2$ ms with at least two catalytic events (5): the cleavage of ATP into ADP and Pi (7) and the release of Pi (14), and finally a $40^\circ$ rapid rotation where the $F_1$ excerts again a torque of 40 pN·nm on the actin filament (7), with the release of ADP at the end (14). Mean rotational frequencies were measured for different actin lengths and ATP concentrations (2), and they constitute valuable comparison data for many theoretical models (15, 16).

The $F_1-$ATPase is constituted, in the simplest functional form, by seven subunits with stoichiometry $\alpha_3\beta_3\gamma$, in which $\alpha$ and $\beta$ subunits are alternately placed to form a cilindrical hexamer (the stator) and the $\gamma$ subunit located in its center (the rotor). From several crystallographic studies it is assumed that $\alpha$ subunits remain almost unchanged, but $\beta$ subunits change through several conformational states. The pioneering models, proposed by the groups of Boyer and (12, 13), Walker (17), and modified by Cross and co-workers (18) involve three conformations for the $\beta$ subunits, all found in crystallographic studies (17): "tight", "loose" and "open", which can be paired with the affinity constants $K_d$ found by Senior et al. (19, 20) of 1 nM, 1 $\mu$M and at least 10 mM for ATP and 40 nM, $1,8\,\mu$M and around 10 mM for ADP, respectively. Another model, proposed initially by Bianchet et al. (21, 22), includes a fourth conformational state, "closed", found also by crystallography, which can be paired with an ATP (ADP) intermediate affinity $K_d$ of $\sim 30\,\mu$M ($\sim 35\,\mu$M), also found by Senior et al. (19, 20).

The importance of this intermediate state has been investigated by experimental (21, 23, 24) and theoretical (25, 26) studies.

What is the role of this fourth conformational state with an intermediate affinity on the rotation of the $F_1-$ATPase molecular motor? Let us assume that, once ATP binds, the $\beta$ subunit *closes* to this intermediate state *before* the rotation of the $\gamma$ subunit. Thus, the affinity constant would remain lower along the $80^\circ$ rotation, the nucleotide would be bound for larger periods of time - pushing the rotation - and the mean rotational frequency would increase, in comparison with a mechanism that goes directly from the "open" to the "tight" conformation along the $80^\circ$ rotation. Specially, this would affect the observed rotational frequency of an actin filament that is propelled by the $F_1-$ATPase molecular motor, just as in the experiments of Yasuda et al. (2). Moreover, the $\gamma$ subunit would rotate the last $40^\circ$ degrees, from the "loose" to the "closed" conformation, before opening and relasing the ADP, just in concordance with the experimental observations of Adachi et al. (14).

The goal of this paper is to investigate this proposal by performing numerical simulations of the rotation of an actin filament when is propelled by the $F_1-$ATPase molecular motor, both with and without the fourth conformational state of intermediate affinity constant, and to compare the results with the experimental data obtained in single-molecule experiments. Our computational approach couples brownian dynamics with a set of kinetic equations to simulate the motion of the actin filament attached of the $F_1$ motor for different actin lenghts and different ATP concentrations, and allows to focus on the kinetic effects of an intermediate affinity in the hydrolysis pathway in a very elegant and simple way. Similar approaches have been conducted by the groups of G. Oster (15, 27, 28), W. Junge (3, 4), and Liu et al. (16) to enhance the length of the simulations up to scales comparable to the period of rotation of the motor. Section 2.1 describes in detail the two hydrolysis mechanisms we used in our simulations, which just differ in the inclusion of the fourth intermediate state for the $\beta$ subunits. Section 2.2 introduces the brownian dynamics method, and section 2.3 developes the kinetic model. Section 2.4 describes how the consumption of ATP by the $F_1-$ATPase motors themselves reduces the ATP avaliable in an amount that becomes relevant at low concentrations. Section 3 shows the results we obtained for the rotation of the actin filament with the 3-State and 4-State pathways and compare them with the single-molecule experiments reported by Yasuda et al. (2). Finally, section 4 summarizes our conclusions.

# 2 Theory

## 2.1 Mechanisms

We have constructed two hydrolysis reaction pathways, which differ from each other only in the presence of the intermediate "closed" conformation for the β subunits. They are based on the four substeps during the 120° catalytic cycle (see Fig. 1).

The 3-State pathway without considering the "closed" conformation is shown in Fig. 1B. Here the β subunits change between three different conformations: "tight" (T), "loose" (L) and "open" (O) (12, 13, 17). Kinetic experiments (19, 20) identified several nucleotide binding affinities that can be paired with these conformations. We will assume in our simulations that ATP (ADP) binds with an affinity constant $K_d$ equal to 1 nM (40 nM) in the T conformation, 1 $\mu$M ($1,8\,\mu$M) in the L conformation and 10 mM ($>10$ mM) in the O conformation. The hydrolysis pathway is divided into four stages. First, ATP binds to the site in the O conformation, and causes a transition towards conformation T. In this process, the β subunit bends in such a way that its upper portion pushes the γ subunit (6, 15, 25, 29), producing an aparent torque of 40 pN·nm (2, 5, 6, 9). Second, once the γ subunit has rotated 80°, the ATP at the site in the conformation T hydrolizes. The energy released by this process is used to induce a conformational change from T to L in this β subunit. This reaction corresponds to the first observed dwell time of 1ms at 80° (5–7). Third, Pi is released at the site in conformation L, taking the other observed 1 ms dwell time at 80°. Actually, the kinetic experiments mentioned above have shown that Pi binds with affinity constants higher than 10 mM to the catalytic site for all conformations of the β subunits (19), and the recent experiments (14) show that this second dwell time changes when Pi concentration is modified. Fourth, once Pi is released, the β subunit opens from L to O, pushing again the γ subunit with an apparent torque of 40 pn·nm and rotating it further 40°. At the end of this cycle, ATP binds to the free site at conformation O, and the opening of the β subunit facilitates the release of ADP, 240° after it bound as ATP (14).

The 4-State pathway considering the "closed" conformation is shown in Fig. 1C. This state, also found by crystallography (21, 23), is much more similar to the T and L conformations than to the O one, and can be associated to the intermediate ATP (ADP) affinity constant of $\sim 30\,\mu$M ($\sim 35\,\mu$M) (19, 20). In this case, the ATP binding drives a local conformational change from O to C, increasing binding affinity and favouring, therefore, the permanence of the nucleotide in the catalytic

site. As a consequence of this process, ATP binding is divided into two substeps: a transition of the β subunit from O to C at 0° before rotating, and a subsequent 80° rotation of the γ subunit together with a conformational change from C to T in the β subunit. The next two steps, ATP hydrolysis and release of phosphate, occur as in the 3-State mechanism. Finally, the ADP release is also divided into two substeps: a 40° rotation of the γ subunit accompanied with a transition from the L to the C conformation and, then, a transition from the C to the O conformation at 120°, that facilitates the release of ADP.

Because we want to focus on the relevance of the "closed" conformational state, both pathways have the same nucleotide occupancies, differing just in the presence or not of the "closed" conformation. We have chosen nucleotide occupances around two (14), but the kinetic equations we derive to perform our simulations does not distinguish between models with nucleotide occupancies of two or three, as can be seen below.

## 2.2 Brownian Dynamics

We used Brownian Dynamics to simulate the rotation of the actin filament attached to the γ subunit (see Fig. 2). Similar approaches have been conducted by the groups of G. Oster (15, 27, 28), W. Junge (3, 4), and by Liu et al. (16) to enhance the length of the simulations up to scales comparable to the period of rotation of the motor. The dimensions of the $F_1$-motor ($\sim$ nm) are negligible compared to the dimensions of the actin filament ($\sim$ $\mu$m) (1, 2). For this reason, we model the actin filament, in first approximation, as a straight bar of length $L$ and radius $r$ inmersed in a viscous fluid (water) and rotating around one end, propelled by the torque produced by the γ subunit of the $F_1-$motor (see Fig. 2). This type of motion can be described by using a rotational Langevin equation (30, 31),

$$I\frac{d\omega}{dt} = -\xi_{\perp}\omega + \lambda(t) + \tau(t) \quad , \tag{1}$$

where $I$ is the moment of inertia and ω is the angular velocity of the rigid body. The first term on the right-hand side of Eq. 1 corresponds to an average frictional viscous torque, with rotational friction coefficient $\xi_{\perp}$. The second term represents a stochastic torque due to the random collision with the solvent molecules and is a rapidily fluctuating function with zero mean. The third term consists in all external torques (30, 31). The first two terms take into account the interactions between the actin filament and the water, and the third therm corresponds to the

torque produced by the $F_1-$motor of approximately 40 pN·nm (2, 6, 9). The rotational friction coefficient in this case is given by (6, 32)

$$\xi_\perp = \frac{4\pi}{3} \cdot \frac{\eta L^3}{\ln(L/r) - 0.447} \quad , \tag{2}$$

where $\eta$ is the viscosity of the medium ($\eta = 10^{-3}$ Nm$^{-2}$ for water at room temperature).

W. F. van Gunsteren and H. J. C. Berendsen (33) developed a third-order algorithm to integrate the Langevin equation for traslational motion. By analogy, we can use the results of this algorithm to obtain the angular position of the rigid body, $\theta$, as a function of time. In the diffusive regime, that is when the friction is so strong that angular velocity $\omega$ relaxes within $\Delta t$ ($I/\xi_\perp \ll \Delta t$), the inertial term (left-hand side of Eq. 1 ) becomes negligible compared to the viscous term (first term on the right-hand side of Eq. 1). The integration algorithm for this case gives (see Eq. 2.27 of W. F. van Gunsteren and H. J. C. Berendsen (33))

$$\theta(t_n + \Delta t) = \theta(t_n) + \frac{1}{\xi_\perp}\left\{\tau(t_n)\Delta t + \frac{1}{2}\dot{\tau}(t_n)(\Delta t)^2\right\} + X_n(\Delta t) \quad , \tag{3}$$

where $\dot{\tau}(t_n)$ is the first time derivate of the torque and $Xn(\Delta t)$ is a random number sampled from a Gaussian distribution with zero mean and width

$$\langle X_n^2(\Delta t)\rangle = \frac{2k_B T}{\xi_\perp}\Delta t \quad , \tag{4}$$

with $k_B$ the Boltzmann constant and $T$ the temperature. Since $F_1-$ATPase rotates at 120° discrete steps, we can restrict the values of $\theta$ between 0° and 120° and impose periodic boundary conditions. The external torque exerted by the $F_1$-motor, $\tau(t_n) = 40$ pN·nm, is set or unset by the kinetic equations as it is described below.

## 2.3 Kinetic equations

Rotational movements of the $\gamma$ subunit are uniquely coupled to the chemical reactions of the catalytic cycle (6, 13, 20, 34–36). During hydrolysis, the first 80° rotation is driven by the binding of ATP and the resting 40° rotation only occurs after the cleavage of ATP and release of phosphate (5, 7, 14). Reaction rates governing these events should be, therefore, function of the angular orientation, $\theta$, of the $\gamma$ subunit (i. e. the reaction coordinate).

$F_1-$ATPase undergoes at least four chemical reaction-states, as depicted in Fig. 3. State 1 waits for the binding of ATP, state 2 for the cleavage of ATP, state 3 for the release of phosphate, and state 4 for the release of ADP. Following a similar approach as presented in references (15, 27, 28, 34–36), we will assume that these chemical reactions are described by a set of coupled kinetic equations:

$$\begin{aligned}
\frac{d[N_1]}{dt} &= -\left(K_T[ATP]+K_D[D]\right)[N_1]+K_{-T}[N_2]+K_{-D}[N_4] \quad , \\
\frac{d[N_2]}{dt} &= K_T[ATP][N_1]-\left(K_{-T}+K_{hyd}\right)[N_2]+K_{syn}[N_3] \quad , \\
\frac{d[N_3]}{dt} &= K_{hyd}[N_2]-\left(K_{syn}+K_{-P}\right)[N_3]+K_P[P][N_4] \quad \textit{and} \\
\frac{d[N_4]}{dt} &= K_D[D][N_1]+K_{-P}[N_3]-\left(K_P[P]+K_{-D}\right)[N_4] \quad , \qquad (5)
\end{aligned}$$

where $[N_i]$ is the concentration of $F_1-$ATPase molecules in the state $i$ ($i$=1,2,3,4) and $[ATP]$, $[D]$ and $[P]$ are the concentration of ATP, ADP and Pi, respectively. Rate constants in the hydrolysis (synthesis) direction are named as follows: the association (dissociation) constant of ATP is $K_T$ ($K_{-T}$), the hydrolysis (synthesis) constant is $K_{hyd}$ ($K_{syn}$), the dissociation (association) constant of Pi is $K_{-P}$ ($K_P$) and the dissociation (association) constant of ADP is $K_{-D}$ ($K_D$).

Let us now assume that $[N_i]$ divided by the total concentration of $F_1$ molecules, $[N]$, is the probability $P_i$ of finding one $F_1$ molecule in the state $i$, $P_i = [N_i]/[N]$. By dividing Eq. 5 by $[N]$, one obtains the following master equation,

$$\frac{d}{dt}\vec{P} = \overrightarrow{K}(\theta)\vec{P}, \qquad (6)$$

where $\vec{P}=:(P_1,P_2,P_3,P_4)^T$ is the vector of probabilities $P_i$, and $\overrightarrow{K}(\theta)$ is a 4×4 matrix given by

$$\overrightarrow{K}(\theta) = \begin{bmatrix} -K_T[ATP]-K_D[D] & K_{-T} & 0 & K_{-D} \\ K_T[ATP] & -K_{-T}-K_{hyd} & K_{syn} & 0 \\ 0 & K_{hyd} & -K_{syn}-K_{-P} & K_P[P] \\ K_D[D] & 0 & K_{-P} & -K_P[P]-K_{-D} \end{bmatrix}. \qquad (7)$$

Eq. (6) can be integrated to calculate $\vec{P}$ at discrete time steps,

$$\vec{P}(t_n+\Delta t) = \vec{P}(t_n)+\overrightarrow{K}(\theta)\vec{P}(t_n)\Delta t. \qquad (8)$$

The reactions only take place within very specific θ intervals (see Fig. 1). We will consider this fact by assuming that the kinetic constants are different from zero only for such angular ranges. Therefore, association and dissociation constants for ATP, Pi and ADP will be different from zero for θ values between 0° and 80°; 79° and 81°, and 80° and 120°, respectively. Consistently, hydrolysis and synthesis constants ($K_{hyd}$ and $K_{syn}$) will be non-zero for θ values between 79° and 81°.

Dissociation constants for ATP, $K_{-T} = K_T \cdot K_d(ATP)$, deserves a special discussion. Driven by the binding of ATP, the β subunit changes from the O conformation at 0° to the T conformation at 80°. This conformational change is gradual along the 80° rotation and caused by the sequential formation of chemical bonds between the ATP and the catalytic site, as proposed in the *binding zipper* model of G. Oster and co-workers (15, 27, 28). In a first approximation the affinity constant for ATP, $K_d(ATP)$, depends exponentially with the free energy difference that drives the closing β subunit, $K_d(ATP) \sim \exp\{-\Delta G_{closing}/k_BT\}$. Since the torque produced by the $F_1-$ATPase is nearly a constant value of 40 pN·nm (7, 9), then $\Delta G_{closing}$ is linearly proportional to θ and $K_d(ATP)$, therefore, will depend exponentially of θ,

$$K_d(ATP) \sim \exp(-A\theta), \tag{9}$$

where $A$, the proportionality constant, can be calibrated from the experimental values of the affinity constants in the different conformations. Fig. 4(a) shows the dependence of $K_d(ATP)$ with θ for the two considered pathways. For the 3-State pathway we assume that $K_d(ATP)$ decreases continuously from from 10 mM at 0° to 1 nM at 80° (blue line). In contrast, for the 4-State pathway, the binding of ATP drives a conformational change of the β subunit from O to C before rotating and, then, from O to T along the 80° rotation. Thus, we will assume in this case that $K_d(ATP)$ abruptly changes from 10 mM to 30 $\mu$M when ATP binds at 0° and, then, it decays exponentially with the rotation from 30 $\mu$M at 0° to 1 nM at 80° (brown line).

Similarly, the dissociation constant for ADP, $K_{-D} = K_D \cdot K_d(ADP)$, is assumed to increase exponentially with θ, from the value in the L conformation at 80° to the value in the O conformation at 120°, as depicted in the Fig. 4(b). For the 3-State pathway, this transition occurs continuously from 1.8 $\mu$M to 10 mM (blue line). For the 4-State pathway, $K_d(ADP)$ increases continuously from 1.8 $\mu$M at 80° to 35 $\mu$M (in the C conformation) at 120°, and then abruptly changes up to 10 mM (brown line). These angular dependencies of the affinity constants constitute the essential differences between both pathways in our simulations.

From all rate constants listed above, the affinity constant for ADP in the O conformation is the only one that has not been measure yet. We will assume a value of 10 mM, similar to the value for the ATP at the same conformation, this reflects the fact that it is almost impossible to find a nucleotide bound in the O conformation (19) (in fact, we have varied this constant from 10 mM to 50 mM, without finding any apparent difference in the simulation results). Also, in the single-molecule experiments of Yasuda et al. (5) two rate constants have been measured for the catalytic processes at 80°: $K_1$ =1640 $s^{-1}$ and $K_2$ =710 $s^{-1}$; but it was not possible to discriminate which one corresponds to the cleavage of ATP, $K_{hyd}$, and which one corresponds to the release of Pi, $K_{-P}$. By performing simulations with both possible assignments, we have not found any significative difference between them. Accordingly, in all simulations we assigned $K_{hyd}$ =1640 $s^{-1}$ and $K_{-P}$ =710 $s^{-1}$. In addition, we will assume that ATP in the T conformation is in equilibrium with ADP+Pi, with an equilibrium constant $K_{eq} \simeq 1$ (22) (that is $K_{syn}$=$K_{hyd}$). The experiments carried out to observe directly the rotation usually contains, in addition to the $F_1$ molecules, an ATP regenerating system consisting of 0.2 mg/ml creatine kinase and 2.5 mM creatine phosphate (2, 5, 9), therefore, concentrations of ADP and Pi are very low compared to the concentration of ATP. In order to compare directly these experiments with our simulations, we will neglect the binding of Pi and ADP. All parameters used in our simulations are summarized in table 1.

## 2.4 Reduction of the ATP concentration

Finally, there is a special feature that is always present but becomes very relevant at low ATP concentrations. Let us assume that $[ATP]_{total}$ is the concentration of ATP molecules deposited initially. $F_1$-motors will convert part of this concentration into $[ADP+Pi]$ and the ATP concentration will be reduced to $ATP = [ATP]_{total} - [ADP+Pi]$. On one hand, the $F_1$-motors consume ATP at a rate of three molecules per turn, and therefore, they decrease the ATP concentration at a rate of $Q_{co} = d[ATP]/dt$=$-3F[F1]$, with $F$ the mean rotational frequency and $[F1]$=10 nM the concentration of $F_1-$ATPase molecules (2). On the other hand, the ATP regenerating system will convert the ADP and Pi back into ATP. Let us assume that this system regenerates ATP with a rate of $Q_{re} = d[ATP]/dt$=$\dot{v}[ADP+Pi]$, where $\dot{v}$ is the fraction of molecules of ADP+Pi converted into ATP per unit time. In equilibrium, the consumption rate equals the

regeneration,$Q_{co} = Q_{re}$, therefore, the ATP concentration reduces to

$$[ATP] = [ATP]_{total} - \alpha F \quad , \tag{10}$$

where and $\alpha$=$3[F1]/\dot{v}$. Because of the efficiency $\dot{v}$ of the regenerating system is unknown, the value for $\alpha$ will be calibrated from the experimental report of the mean rotational frequency at the lowest ATP concentration value of 10 nM for an actin filament of length 1 $\mu$m.

The feature mentioned above raises a new question: given an ATP concentration, the simulation yields a mean rotational frequency $F$, but $[ATP]$ itself is a function of $F$ (Eq. 10). Let us call $F_{in}$ the frequency we choose to compute the ATP concentration, and $F_{out}$ the rotational frequency given out from the simulation. We handled this issue by imaging the difference between the output frequency $F_{out}$ and the input frequency $F_{in}$ as a function of $F_{in}$, $\Delta F(F_{in}) = F_{out} - F_{in}$, that can be searched for a root by the bisection method (37, pp. 153-166). Such root is the final frequency predicted by our model for the initial concentration $[ATP]_{total}$. We have generated ten trajectories for each $[ATP]_{total}$ with different random seeds. We have calculated a value for the output frequency, $F_{out}$, from each one of these trajectories, as the slope of the curve of number of revolutions vs. time. Then, these values were averaged to obtain the mean rotational frequency. The error of this value was calculated as $\Delta F/2$ in the last iteration step of the bisection method.

# 3 Results

First, in order to test the brownian dynamics algorithm (without kinetic equations), a simulation of a rigid bar of length $L = 2.6$ $\mu$m and radius $r = 5$ nm was developed, inmersed in water (with viscosity, $\eta = 10^{-3}$ N·s·m$^{-2}$) and rotating around one end (see Fig. 2). Since the motion is restricted to the *xy* plane, the average of the second Legendre polynomial of the Cosine of the rotated angle goes to a constant value when $t \to \infty$ (31),

$$\lim_{t\to\infty} \langle P_2(\cos\theta)\rangle = \left\langle P_2\left[\cos\left(\frac{\pi}{2}\right)\right]\right\rangle^2 = 0.25, \tag{11}$$

where $\pi/2$ is the angle subtended between the bar and the *z* axis. The rotational trajectory was generated at discrete time steps, $\Delta t = 1\times10^{-6}$ s. The curve of $\langle P_2(\cos\theta)\rangle$ as a function of time is shown in Fig. 5. It can be seen that this average goes to 0.25, in concordance with the Eq. 11. In addition, the inset of

the Fig. 5 shows the first $1\times10^{-5}$ s with a smaller time step, $\Delta t = 1\times10^{-8}$ s (solid line), in good agreement with the results from the software *Brownrig*, designed by the group of de la Torre et.al. (31) (dotted line). These results show us that the brownian dynamics algorithm accurately reproduces the actual rotational diffusion.

Second, we calibrated the $\alpha$ constant of Eq. 10 for both the 3-State and the 4-State mechanisms, which describes the reduction of the ATP concentration as a consequence of the ATP consumption by the $F_1-$ATPase motors themselves. The values that best fit the experimental frequency of 0.1 Hz for an actin filament of 1 $\mu$m at an ATP concentration of 10 nM are $\alpha$=$0.56\times10^{-7}$ Ms and $\alpha$=$1.2\times10^{-7}$ Ms for the 3-State mechanism and the 4-State mechanism, respectively. Once $\alpha$ is known, we can compute the mean rotational frecuencies for different values of $[ATP]_{total}$ by using the bisection method described in the previous section. It was necessary to perform between five and ten bisection iterations to obtain values with uncertainties between 0.5% and 3.5%.

Fig. 6 shows typical rotational trajectories obtained with different random seeds, during the last iteration step of the bisection method, for different $ATP_{total}$ concentrations. Curves show a systematic reduction of the rotational rate in the 3-State pathway (black lines) compared to the 4-State mechanism (grey lines), which is conserved in a wide range of $ATP_{total}$ concentrations down to nanomolar to milimolar. Rotational rates can be obtained from the slope of each one of these curves, and then they are averaged to obtain the output mean rotational frequency, $F_{out}$. The insets, showing the average over the ensamble of trajectories, confirm the difference in the rotational activity for both pathways.

Third, the results of including or not the reduction of the ATP concentration are shown in Fig. 7. For both pathways, the effect of the ATP reduction becomes only appreciable at low concentrations ($[ATP] < 2\times10^{-7}$ M), and induces a better agreement with the experimental values in this $[ATP]$ range. Note that this effect is a feature of the experimental setup and not an intrinsic property of the $F_1-$ATPase molecular motor.

Now, we investigate the differences in the predictions of the 3-State and the 4-State pathways. Fig. 8 shows the computed mean rotational frequency as a function of the actin length for different ATP concentrations. Both models predict the decreasing of the frequency as the length of the filament increases. For $[ATP]_{total}$=2 mM there is not a clear difference between both models. Nevertheless, for lower concentrations the 3-State values become lower than the 4-State values, which are much closer to the experimental data. Fig. 9 shows the mean rotational frequency as a function of the ATP concentration for an actin filament

of length $1\mu$m. The agreement of the 4-State values with the experimental curve is excellent; in constrast, the 3-State mechanism gives values that are systematically lower than observed. By fitting the frequency values to the expression (2)

$$F = \frac{F_{max}[ATP]_{total}}{[ATP]_{total} + K_{1/2}} \quad , \tag{12}$$

we found for the 4-State model that $F_{max} = 3.69$ Hz and $K_{1/2} = 0.75$ $\mu$M (dotted line), which differ from the experimental values ($F_{max} = 3.9$ Hz and $K_{1/2} = 0.8$ $\mu$M (2)) in 7.0% and 6.5%, respectively. In contrast, the same fit for the 3-State mechanism gives $F_{max} = 2.0$ Hz and $K_{1/2} = 0.36$ $\mu$M (dashed line), which differ from the experimental values in 48.6% and 55.3%, respectively. These results show that the affinity constants for ATP binding are too low in the 3-State mechansims to reproduce the rotational frequency caractheristics, as will be discussed in the conclusions.

# 4 Conclusions

Hereby we have investigated two different mechanism already proposed for the synthesis of the $F_1$-ATPase via a computer simulation. We have carefully considered all the necessary experimental data to perform this study. The simulation uses brownian dynamics for the angular displacemet plus a reduced set of four kinetic equations for the chemical reactions that take place in the mechanism. Both mechanisms have been implemented to simulate the rotation of an actin filament propelled by the $F_1-$ATPase, and their results have been compared with the experimental reports of Yasuda et al. (2). Our simulations show that the 4-State pathway reproduces extraordinary well the measured frequencies for all ATP concentrations (20nM to 20mM) and all filament lengths (0.5 $\mu$M to 4 $\mu$M). In contrast, the 3-State pathway gives frequencies that are systematically lower than observed at high ATP concentrations.

We have focus our attention in particular to the main differences between the two mechanisms, namely the "closed" conformational state and its intermediate nucleotide affinity.

Where do these differences between the rotational frequencies of both pathways come from? The answer can be found in the first 80° rotation. In the 3-State pathway (see Fig. 4), the $\beta$ subunit changes directly from the O conformation to the T conformation along the rotation of the $\gamma$ subunit, and the affinity constant $K_d$ for ATP drops exponentially from 10 mM at 0° to 1 nM at 80°. In the 4-State

pathway, in contrast, the β subunit goes from the O conformation to the C conformation before the γ subunit rotates, and then β changes from C to T along the rotation of γ. The affinity constant for ATP changes exponentially from 30 $\mu$M at 0° to 1 nM at 80°, i. e., with values that are three orders of magnitude lower than in the 3-State pathway. Thus, the probability of ATP to release at any point between 0° and 80° is much higher in the 3-State pathway than in the 4-State one. Since the effective torque of 40 pN·nm is only exerted if the nucleotide is bound to the β subunit, the release of ATP actually stops the rotation until a new ATP binds, and this event occurs more often in the 3-State pathway than in the 4-State one. In consequence, the 3-State pathway shows a lower mean rotational frequency, and this difference dissapears at high ATP concentrations.

A similar difference between the ADP affinity constant in the 40° substep in both pathways (see Fig. 4(b)) would be crucial in the synthesis direction ( i.e., from the right to the left in Fig. 1), but this difference does not affect the rotational frequency in the hydrolysis. Indeed, by using the 4-State pathway we replaced the angular dependency of $K_{dD}$ for ADP from the curve depicted in brown to the curve depicted in blue in the Fig. 4(b), and we did not observe any change in the computed values (data not shown). This is just because the 40° rotation and the setting of an effective torque of 40 pN·nm are triggered by the release of Pi, and not by the presence or absence of a bound ADP at the β subunit.

There is, however, an important effect concerning the angle of ADP release. In the 3-State pathway the affinity constant $K_{dD}$ for ADP exponentially grows from 1.8 $\mu$M in the L conformation at 80° to around 10mM in the O conformation at 120°, and thus ADP can be released everywhere between 80° and 120°. In the 4-State pathway, in contrast, $K_{dD}$ exponentially grows from 1.8 $\mu$M in the L conformation at 80° to 35 $\mu$M in the C conformation at 120°, and then the β subunit opens to the O conformation ($k_{dD}$ around 10 mM) just at 120°. Thus, the ADP is only released at 120° in the 4-State mechanism. This agrees with the experimental observations of Adachi et al. (14), and avoids ATP to bind the β subunit where ADP is located. Indeed, Adachi et al. (14). have observed that ADP is released *after* a new ATP is bound. This fact, together with the differences on the mean rotational frequencies between the 3-State and the 4-State pathways described above emphasize the relevance of the “closed ”intermeadiate conformation on the function of the $F_1-$ATPase molecular motor.

As an additional result, we have found that the efficiency of the regenerating system in the experimental setup of Yasuda et al. (2) plays a significative role on the mean rotational frequency of the actin filament at low ATP concentrations. In fact, the actual ATP concentration that is ready to react with a single

$F_1-$ATPase motor shows to be lower than the initial value set in the experiment, because there are so few molecules at nM concentrations that those consumed by the $F_1-$ATPase motors must to be taken into account. In equilibrium, the regenerating rate equals the consumption rate, and such actual ATP concentration can be obtained from the efficiency of the regenerating system, but this value is unknown. Once this efficiency is obtained from the calibration of a first experimental point, all rotational frequencies obtained from the simulation of the 4-State mechanism reproduces the experimental data, but not the 3-State mechanism, which gives significatively lower values.

We have simulated the functional mechanism of the $F_1-$ATPase molecular motor in the hydrolysis direction, however the same methodology can be applied in future studies for the synthesis mechanism. For this purpose we suggest to simulate the rotation of gold beads attached to the $\gamma$ subunit, propeled in the clockwise direction by an external magnetic field. These experiments have been performed by Itoh et al. (8), and the ATP production rate measured there can be compared with future simulation results. Recently has been suggested that $F_1-$ATPase can operate through (at least) two competing reaction pathways (10). This new kind of mechanism can be also studied with the computational approach introduced in this work, just by modifying the kinetic equations.

# 5 Acknowledgments

We thank T. Dittrich for his invitation to work with in the project *Driven Transport Phenomena in electronic and biological nanosystems* and L. M. Amzel and M. A. Bianchet for their unvaluable comments and suggestions. We also thank K. Adachi and H. Nakamura for useful discussions, and W. Oquendo for carefully reading the manuscript. A preliminary version of this work was exhibited as a poster in the $52^{th}$ Annual Meeting of the Biophysical Society and $16^{th}$ IUPAB International Biophysics Conference (Long Beach, CA, 2008) and deserved a travel award, and we are very grateful for this support. This research was supported by COLCIENCIAS (project number 1101-05-17608), and the Bogota Research Division (DIB) of the National University of Colombia. The simulation of physical systems group of the National University of Colombia is part of the Center for Basic and Interdisciplinary Studies in Complexity, CeiBA - Complejidad. J. A. Leyva was supported by National Institutes of Health (NIH) grant GM 066895 (to L. Mario Amzel).

# References


1. Noji, H., R. Yasuda, M. Yoshida, and K. Kinosita, 1997. Direct observation of the rotation of $F_1-$ATPase. *Nature* 386:299–302.

2. Yasuda, R., H. Noji, K. Kinosita, and M. Yoshida, 1998. $F_1$-ATPase is a highly efficient molecular motor that rotates with discrete 120° steps. *Cell* 93:1117–1124.

3. O.Pänke, D. Cherepanov, K. Gumbiowski, S. Engelbrecht, and W. Junge, 2001. Viscoelastic Dynamics of Actin Filaments Coupled to Rotary F-ATPase: Angular Torque Profile of the Enzyme. *Biophys. J.* 81:1220–1233.

4. Cherepanov, D., and W. Junge, 2001. Viscoelastic Dynamics of Actin Filaments Coupled to Rotary F-ATPase: Curvature as an Indicator of the Torque. *Biophys. J.* 81:1234–1244.

5. Yasuda, R., H. Noji, M. Yoshida, K. Kinosita, and H. Itoh, 2001. Resolution of distinct rotational substeps by submillisecond kinetic analysis of $F_1$-ATPase. *Nature* 410:898–904.

6. Kinosita, K., K. Adachi, and H. Itoh, 2004. Rotation of $F_1$-ATPase: How an ATP-Driven Molecular Machine May Work. *Annu. Rev. Biophys. Biomol. Struct.* 33:245–268.

7. Shimabukuro, K., R. Yasuda, E. Muneyuki, K. Hara, K. Kinosita, and M. Yoshida, 2003. Catalysis and rotation of $F_1$ motor: cleavage of ATP at the catalytic site occurs in 1 ms before 40° substep rotation. *Proc. Natl. Acad. Sci.* 100:14731–14736.

8. Itoh, H., A. Takahashi, K. Adachi, H. Noji, R. Yasuda, M. Yoshida, and K. Kinosita, 2004. Mechanically driven ATP synthesis by $F_1$-ATPase. *Nature* 427:465–468.

9. Sakaki, N., R. Shimo-Kon, K. Adachi, H. Itoh, F. S, E. Muneyuki, M. Yoshida, and K. Kinosita, 2005. One rotary mechanism for $F_1$-ATPase over ATP concentrations from millimolar down to nanomolar. *Biophys. J.* 88:2047–2056.

10. Shimabukuro, K., E. Muneyuki, and M. Yoshida., 2006. An alternative reaction pathway of $F_1$-ATPase suggested by rotation without $80°/40°$ substeps of a sluggish mutant at low ATP. *Biophys. J.* 90:1028–1032.

11. Ueno, H., T. Suzuki, K. Kinosita, and M. Yoshida, 2005. ATP-driven stepwise rotation of $F_0F_1$-ATP synthase. *Proc. Natl. Acad. Sci.* 102:1333–1338.

12. Boyer, P., 1993. The binding change mechanism for ATP synthase–some probabilities and possibilities. *Biochimica et biophysica acta* 1140:215.

13. Boyer, P., 1997. The ATP synthase - a splendid molecular machine. *Annu. Rev. Biochem.* 66:717–749.

14. Adachi, K., K. Oiwa, T. Nishizaka, S. Furuike, H. Noji, H. Itoh, M. Yoshida, and K. Kinosita, 2007. Coupling of Rotation and Catalysis in $F_1-ATPase$ revealed by single-molecule imaging and manipulation. *Cell* 130:309–321.

15. Wang, H., and G. Oster, 1998. Energy transduction in the F1 motor of ATP synthase. *Nature* 396:279–282. `http://dx.doi.org/10.1038/24409`, 10.1038/24409.

16. Liu, M. S., B. D. Todd, and R. J. Sadus, 2003. Kinetics and chemomechanical properties of the F[sub 1]-ATPase molecular motor. *The Journal of Chemical Physics* 118:9890–9898. `http://link.aip.org/link/?JCP/118/9890/1`.

17. Abrahams, J. P., A. G. Leslie, R. Lutter, and J. E. Walker, 1994. Structure at 2.8 Å resolution of $F_1$-ATPase from bovine heart mitochondria. *Nature* 370:621–628.

18. Duncan, T., V. Bulygin, Y. Zhou, M. Hutcheon, and R. Cross, 1995. Rotation of subunits during catalysis by *Escherichia coli* $F_1$-ATPase. *Proc. Natl. Acad. Sci. USA* 92:10964–10968.

19. Weber, J., and A. E. Senior, 1997. Catalytic mechanism of $F_1$-ATPase. *Biochim. Biophys. Acta* 1319:19–58.

20. Senior, A. E., S. Nadanaciva, and J. Weber, 2002. The molecular mechanism of ATP synthesis by $F_1F_0$-ATP synthase. *Biochim. Biophys. Acta* 1553:188–211.

21. Bianchet, M. A., J. Hullihen, P. L. Pedersen, and L. M. Amzel, 1998. The 2.8-Å structure of rat liver $F_1$-ATPase: Configuration of a critical intermediate in ATP synthesis/hydrolysis. *Proc. Natl. Acad. Sci.* 95:11065–11070.

22. Bianchet, M., P. Pedersen, and L. Amzel, 2000. Notes on the mechanism of ATP synthesis. *Journal of Bioenergetics and Biomembranes* 32:517–521.

23. Menz, R., J. Walker, and A. Leslie, 2001. Structure of Bovine Mitochondrial $F_1$-ATPase with Nucleotide Bound to All Three Catalytic Sites: Implications for the Mechanism of Rotary Catalysis. *Cell* 106:331–341.

24. Chen, C., A. Saxena, W. Simcoke, D. Garboczi, P. Pedersen, and Y. Ko, 2006. Mitochondrial ATP synthase: crystal structure of the catalytic $F_1$ unit in a vanadate-induced transition-like state and implication for mechanism. *J. Biol. Chem.* 281:13777–13783.

25. Böckmann, R., and H. Grubmüller, 2003. Conformational dynamics of the $F_1$-ATPase $\beta-$Subunit: a molecular dynamics study. *Biophys. J.* 85:1482–1491.

26. Leyva, J., M. Bianchet, and L. Amzel, 2003. Understanding ATP synthesis: structure and mechanism of the F1-ATPase (Review). *Molecular membrane biology* 20:27–33.

27. Oster, G., and H. Wang, 2000. Reverse engineering a protein: the mechanochemistry of ATP synthase. *Biochimica et Biophysica Acta (BBA) - Bioenergetics* 1458:482–510. http://www.sciencedirect.com/science/article/B6T1S-40CRY7P-S/1/b7ffcfdcbd23a

28. Sun, S. X., H. Wang, and G. Oster, 2004. Asymmetry in the F1-ATPase and Its Implications for the Rotational Cycle. *Biophys. J.* 86:1373–1384. http://www.biophysj.org/cgi/content/abstract/86/3/1373.

29. G. Pérez-Hernández, E. García-Hernández, RA Zubillaga, and MT de Gómez-Puyou, 2002. Structural energetics of MgADP binding to the isolated beta subunit of $F_1$-ATPase from thermophilic Bacillus PS3. *Arch Biochem Biophys.* 408:177–183.

30. W. T. Coffey, J. P. Kalmykov, and A. V. Titov, 2002. Langevin equation method for the rotational brownian motion and orientational relaxation in liquids. *J. Phys. A: Math. Gen.* 35:6789–6803.

31. Fernandes, M. X., and J. G. de la Torre, 2002. Brownian dynamics simulation of rigid particles of arbitrary shape in external fields. *Biophys. J.* 83:3039.

32. K. Adachi, H. Noji, and K. Kinosita Jr., 2003. Single-Molecule imaging of rotation of $F_1$-ATPase. *Methods Enzymol.* 361:211–227.

33. W. F. van Gunsteren, and H. J. C. Berendsen, 1982. Algorithms for brownian dynamics. *Mol. Phys.* 45:637–647.

34. Gao, Y. Q., W. Yang, R. A. Marcus, and M. Karplus, 2003. A model for the cooperative free energy transduction and kinetics of ATP hydrolysis by F 1 -ATPase. *Proceedings of the National Academy of Sciences of the United States of America* 100:11339–11344. `http://www.pnas.org/content/100/20/11339.abstract`.

35. Yang, W., Y. Q. Gao, Q. Cui, J. Ma, and M. Karplus, 2003. The missing link between thermodynamics and structure in F 1 -ATPase. *Proceedings of the National Academy of Sciences of the United States of America* 100:874–879. `http://www.pnas.org/content/100/3/874.abstract`.

36. Gao, Y. Q., W. Yang, and M. Karplus, 2005. A structure-based model for the synthesis and hydrolysis of ATP by $F_1$-ATPase. *Cell* 123:195–205.

37. W. T. Vetterling, S. A. Teukolsky, W. H. Press, and B. P. Flannery, 2002. Numerical Recipes. Example Book (C++). Cambridge University Press, second edition.

38. Gibbons, C., M. Montgomery, A. Leslie, and J. E. Walker, 2000. The structure of the central stalk in bovine $F_1$-ATPase at 2.4 Å resolution. *Nat. Struct. Biol.* 7:1055–1061.

| | |
|---|---|
| Time step: | $\Delta t = 1 \times 10^{-7}$ s |
| Temperature: | $T = 298$ K |
| Water viscosity: | $\eta = 10^{-3}$ N·s·m$^{-2}$ |
| ATP association constant: | $K_T = 2 \times 10^7 \mathrm{M}^{-1}\mathrm{s}^{-1}$ |
| ATP dissociation constant: | $K_{-T} = K_T \cdot K_d(ATP)$, function of $\theta$ |
| ATP affinity constants: | $K_d(ATP) = \begin{cases} 10 \text{ mM} & \text{in the O conformation} \\ 30\ \mu\text{M} & \text{in the C conformation} \\ 1 \text{ nM} & \text{in the T conformation} \end{cases}$ |
| ADP association constant: | $K_D = 5 \times 10^5 \mathrm{M}^{-1}\mathrm{s}^{-1}$ |
| ADP dissociation constant : | $K_{-D} = K_D \cdot K_d(ADP)$, function of $\theta$ |
| ADP affinity constants: | $K_d(ADP) = \begin{cases} 1.8\ \mu\text{M} & \text{in the L conformation} \\ 35\ \mu\text{M} & \text{in the C conformation} \\ 10 \text{ mM} & \text{in the O conformation} \end{cases}$ |
| Pi association constant: | $K_P = 0$, |
| Pi dissociation constant: | $K_{-P} = 710\ \mathrm{s}^{-1}$ |
| ATP hydrolysis and synthesis constants: | $K_{hyd} = K_{syn} = 1640\ \mathrm{s}^{-1}$ |

Table 1: Simulation parameters

# Figure Legends

**Figure 1.**

(A) Squematic representation of the 120° rotational step according to (14). Vertical axis is the angle rotated by the γ subunit and the horizontal axis is the time. (B) Hydrolysis pathway for the 3-State mechanism. (C) Hydrolysis pathway for the 4-State mechanism. The circles represent different conformations of the $F_1-$ATPase. Each portion represents one α and one β subunit, in one of the following four conformational states: open (O), loose (L), tight (T) and closed (C). The angular position of the γ subunit is indicated by the center arrow.

**Figure 2.**

Actin filament attached to the γ subunit of the $F_1$-motor (not to scale). The dimensions of the $F_1$-motor ($\sim$ nm) are negligible compared with the dimensions of the actin filament ($\sim$ $\mu$m) (1, 2). For this reason, we model the actin filament, in first approximation, as a straight bar of length $L$ and radius $r$ rotating around one end. The $F_1-$ATPase was drawn with Rasmol using the crystal structure 1E79 from the PDB (38).

**Figure 3**

Sequence of catalytic events that takes place during hydrolysis. Note that this sequence represents both mechanisms, and all the possible conformations for the β subunits are not shown explicitly. Nevertheless, the conformations are included in the values of the affinity constants $K_d$. Numbers indicate the possible conformational states. Rate constants of all possible chemical reactions are also shown.

**Figure 4**

Affinity constants, $K_d$, as a funtion of the angle θ in both the 3-State and the 4-State mechanisms for a) ATP between 0° and 80° and b) ADP between 80° and 120°. In the 3-State mechanism (blue lines) the β directly changes from O at 0° to T at 80° and from L at 80° to O at 120° along the rotation. In the 4-State mechanism (brown lines) the β subunit closes to configuration C at 0° before rotation and opens from C at 120° after rotation.

**Figure 5**

Average of the second Legendre polynomial of the Cosine of the rotation angle, $\langle P_2(\cos\theta)\rangle$, as a function of the time. The inset shows the first $1\times10^{-5}$ s with a smaller time step, $\Delta t = 10^{-8}$ s, by using both the algorithm of W. F. van Gunsteren and H. J. C. Berendsen (33) (solid line), and the software *Brownrig* designed by the group of de la Torre (31) (dotted line).

**Figure 6**

Typical rotational trajectories obtained with different random seeds, during the last iteration step of the bisection method, for different $ATP_{total}$ concentrations. Black and grey curves correspond to the 3-State and the 4-State pathway, respectively. The inset shows the average of the ensemble of trajectories for both models.

**Figure 7**

Mean rotational frequency as a function of the total ATP concentration $[ATP]_{total}$ for an actin filament of length $L = 1$ $\mu$m with (filled circles) and without (open circles) the $[ATP]$ reduction given by Eq. 10, for both, a), the 3-State and, b), the 4-State pathways. Experimental data (squares) were obtained from Yasuda et al. (2). The solid line shows the fit $F = F_{max}[ATP]_{total}/([ATP]_{total}+K_{1/2})$ for the experimental data, where $F_{max} = 3.9$ Hz and $K_{1/2} = 0.8$ $\mu$M (2).

**Figure 8**

Mean rotational frecuency vs. actin length at several ATP concentrations, for both the 3-State mechanism (open circles) and the 4-State mechanism (filled circles). The experimental data (squares) are taken from (2).

**Figure 9**

Mean rotational frecuency vs. total ATP concentration, $ATP_{total}$, for both the 3-State mechanism (open circles) and the 4-State mechanism (filled circles). The experimental data (squares) are taken from (2). The lines are fittings of Eq. 12 (2) to the experimental data (solid line), the 3-State mechanism data (dashed line) and the 4-State mechanism data (dotted line). The actin length is $L = 1$ $\mu$m.

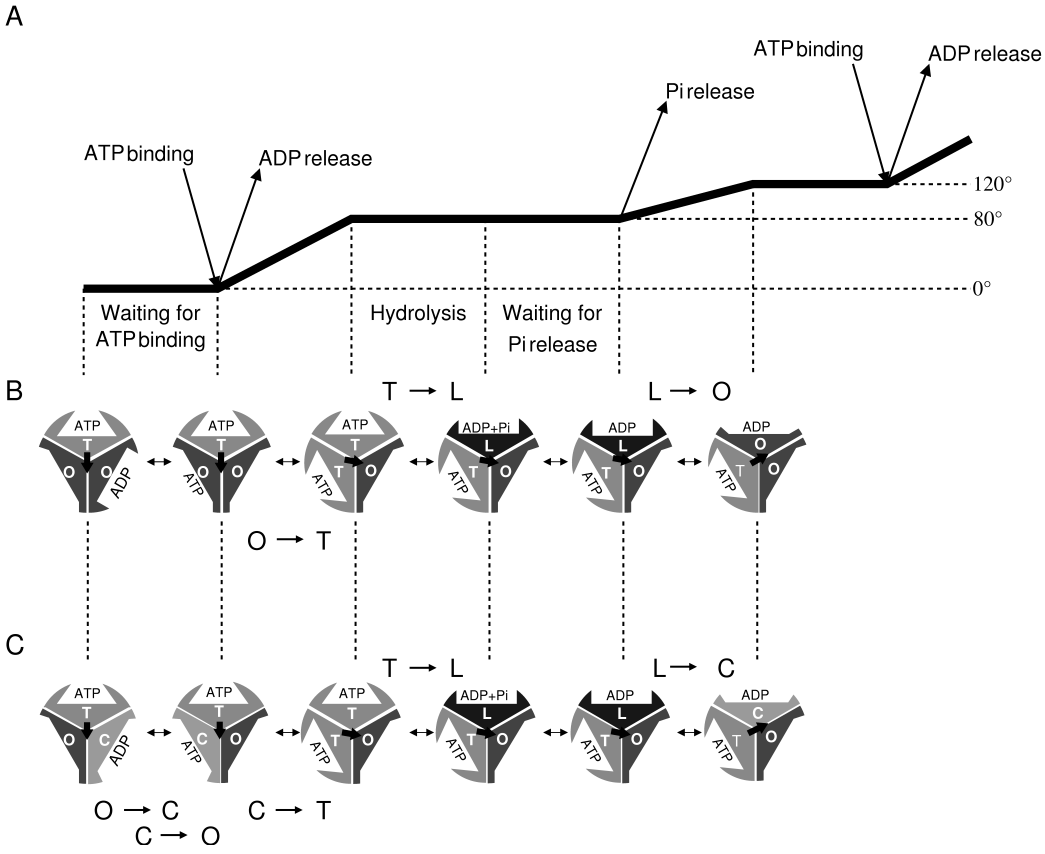
A
ATP binding
ADP release
Pi release
ATP binding
ADP release
120°
80°
0°
Waiting for ATP binding
Hydrolysis
Waiting for Pi release
B
T → L
L → O
O → T
C
T → L
L → C
O → C
C → T
C → O

Figure 1

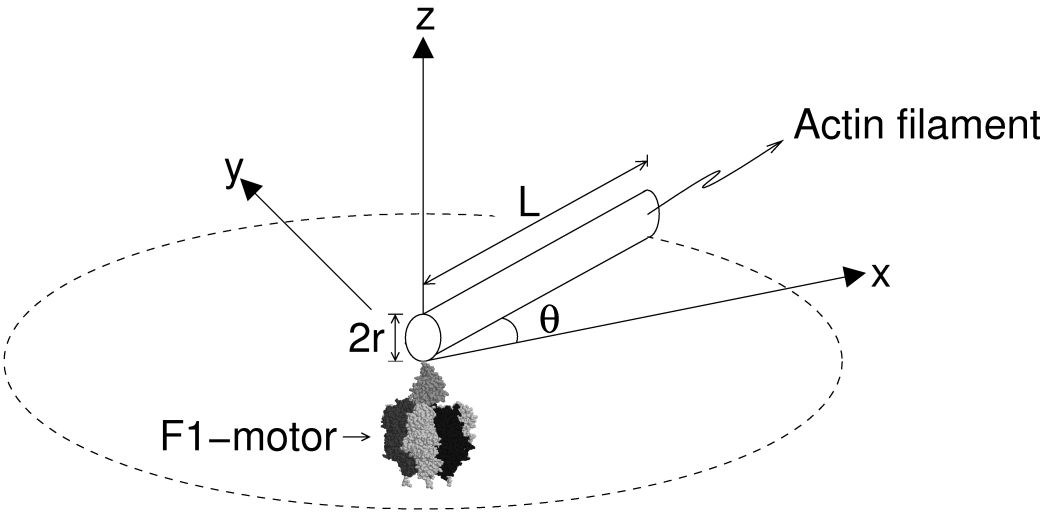


Figure 2

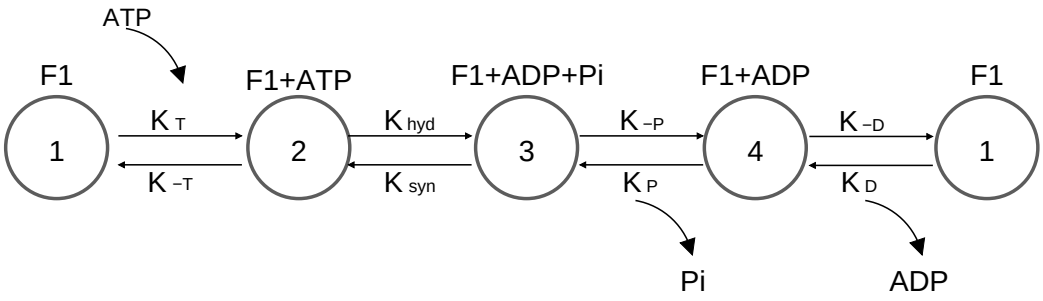
ATP
F1
F1+ATP
F1+ADP+Pi
F1+ADP
F1
1
2
3
4
1
K T
K −T
K hyd
K syn
K −P
K P
K −D
K D
Pi
ADP

Figure 3

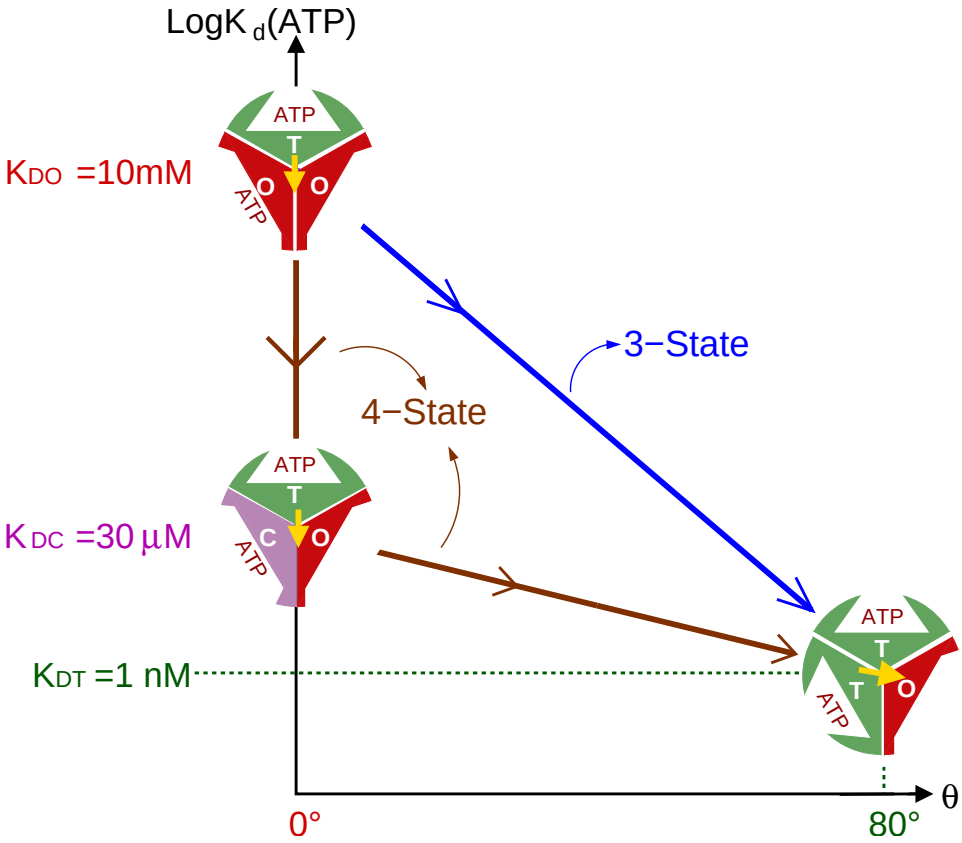


(a) $K_d$ for ATP

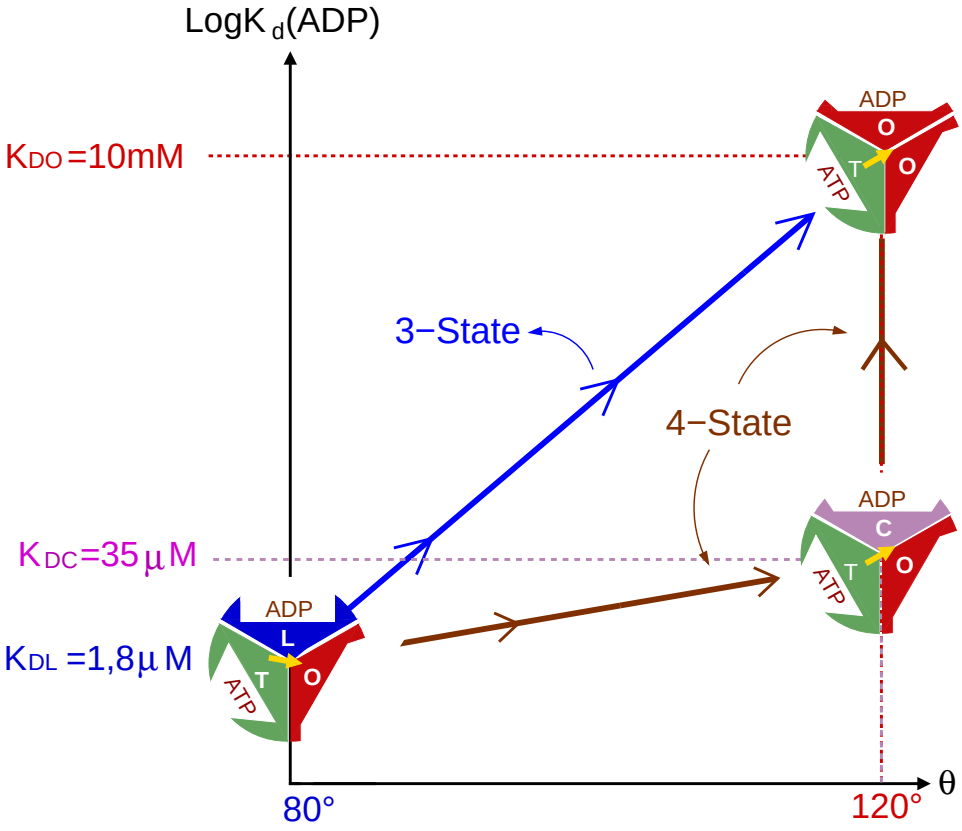


(b) $K_d$ for ADP

Figure 4

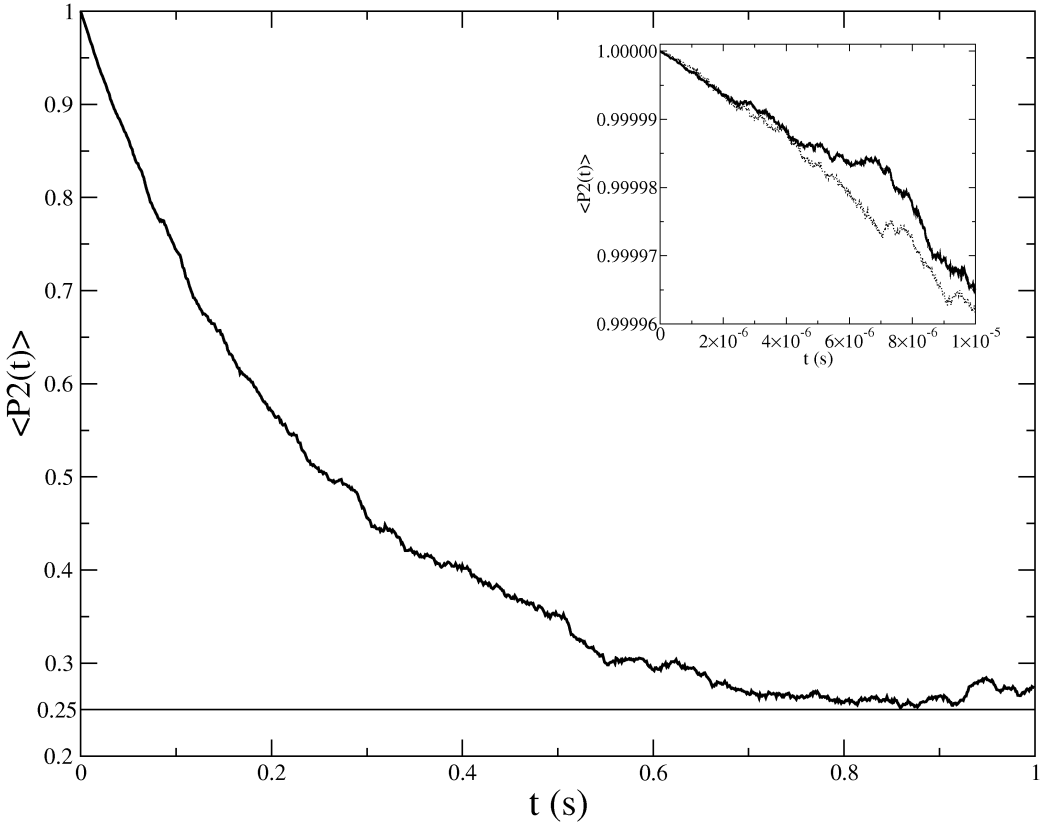
<P2(t)>
t (s)
1
0.9
0.8
0.7
0.6
0.5
0.4
0.3
0.25
0.2
0
0.2
0.4
0.6
0.8
1
1.00000
0.99999
0.99998
0.99997
0.99996
2×10-6
4×10-6
6×10-6
8×10-6
1×10-5

Figure 5

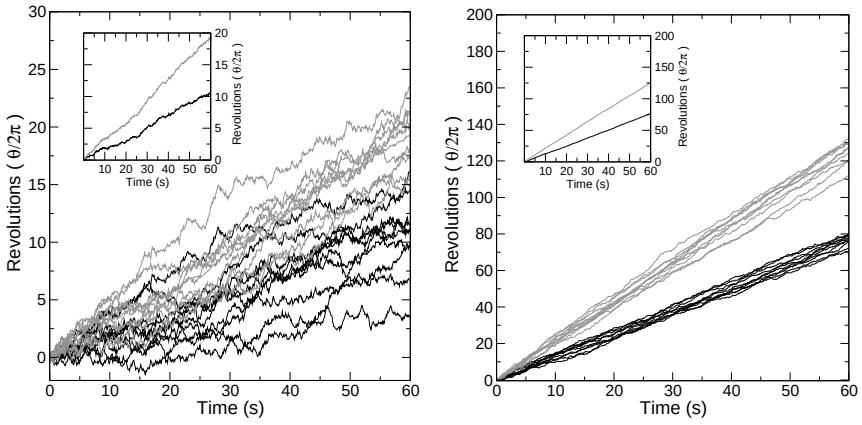


(a) $[ATP]_{total} = 0.06\ \mu$M (b) $[ATP]_{total} = 2\ \mu$M

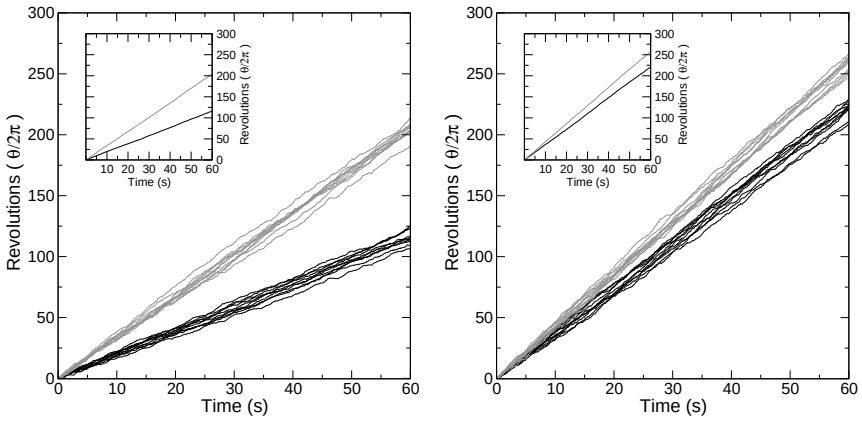


(c) $[ATP]_{total} = 20\ \mu$M (d) $[ATP]_{total} = 2$ mM

Figure 6

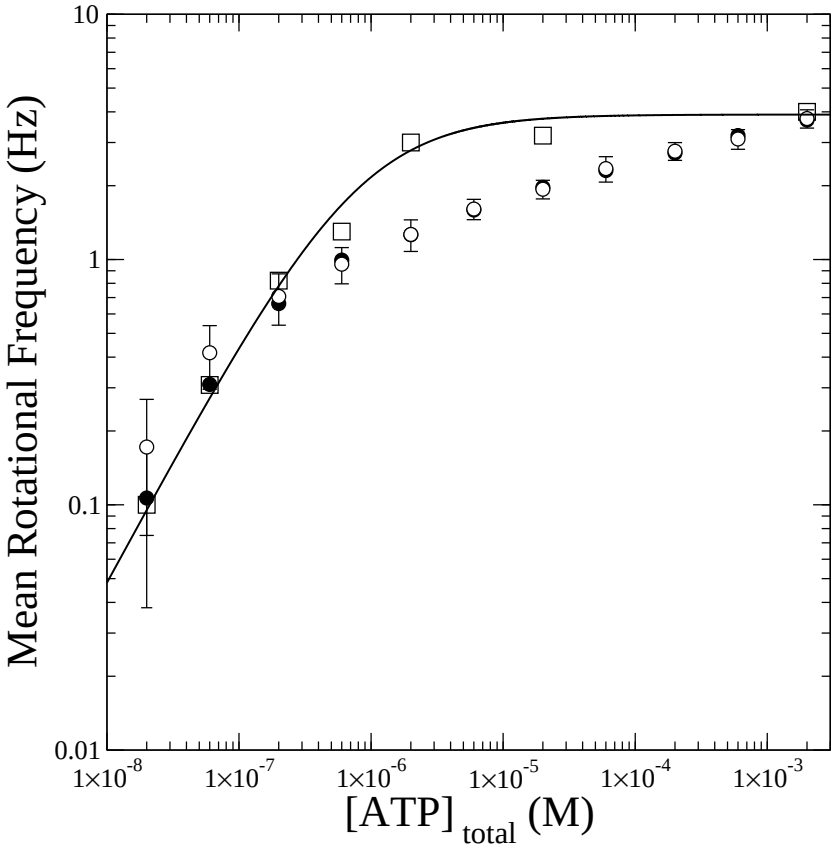


(a) 3-State mechanism

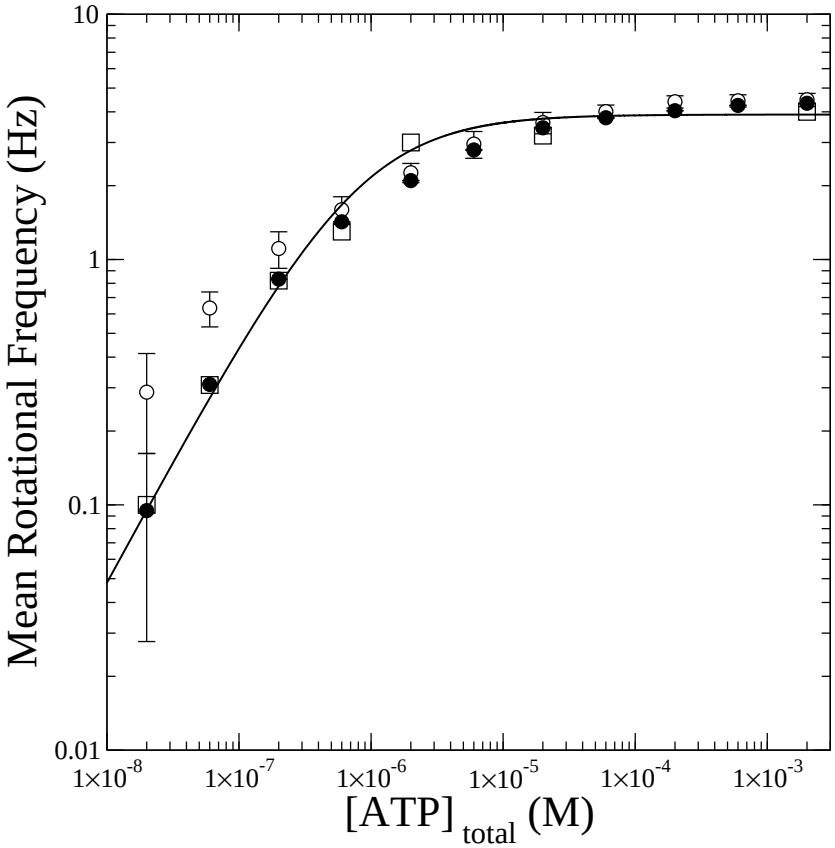


(b) 4-State mechanism

Figure 7

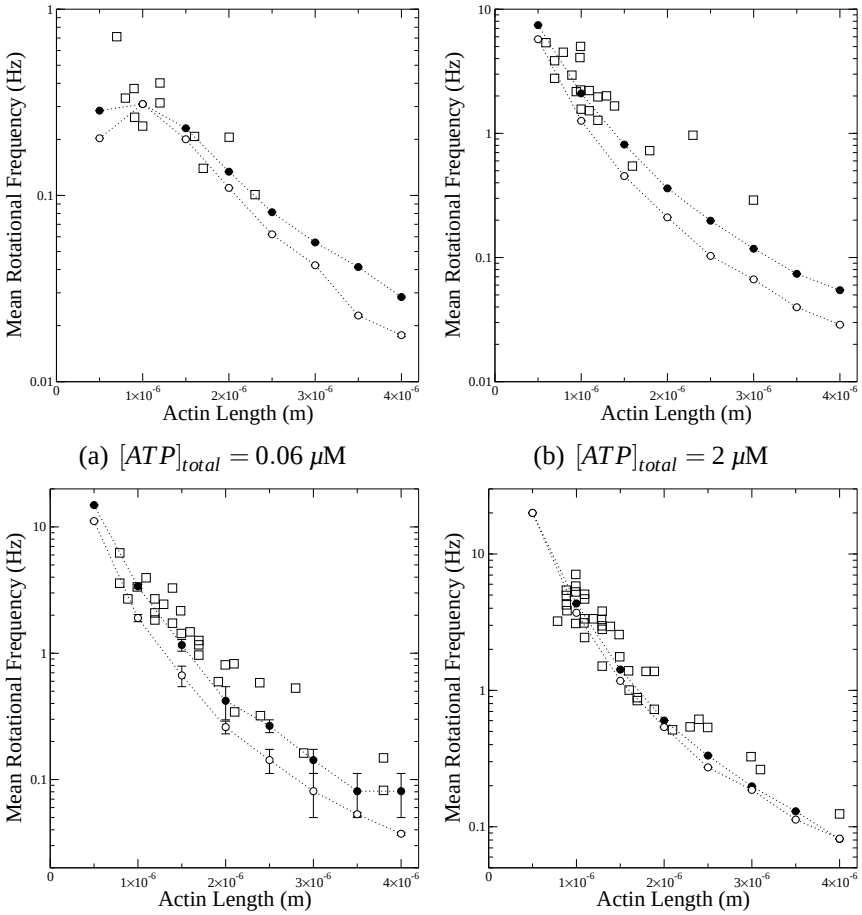


(a) $[ATP]_{total} = 0.06\ \mu$M (b) $[ATP]_{total} = 2\ \mu$M

(c) $[ATP]_{total} = 20\ \mu$M (d) $[ATP]_{total} = 2$ mM

Figure 8

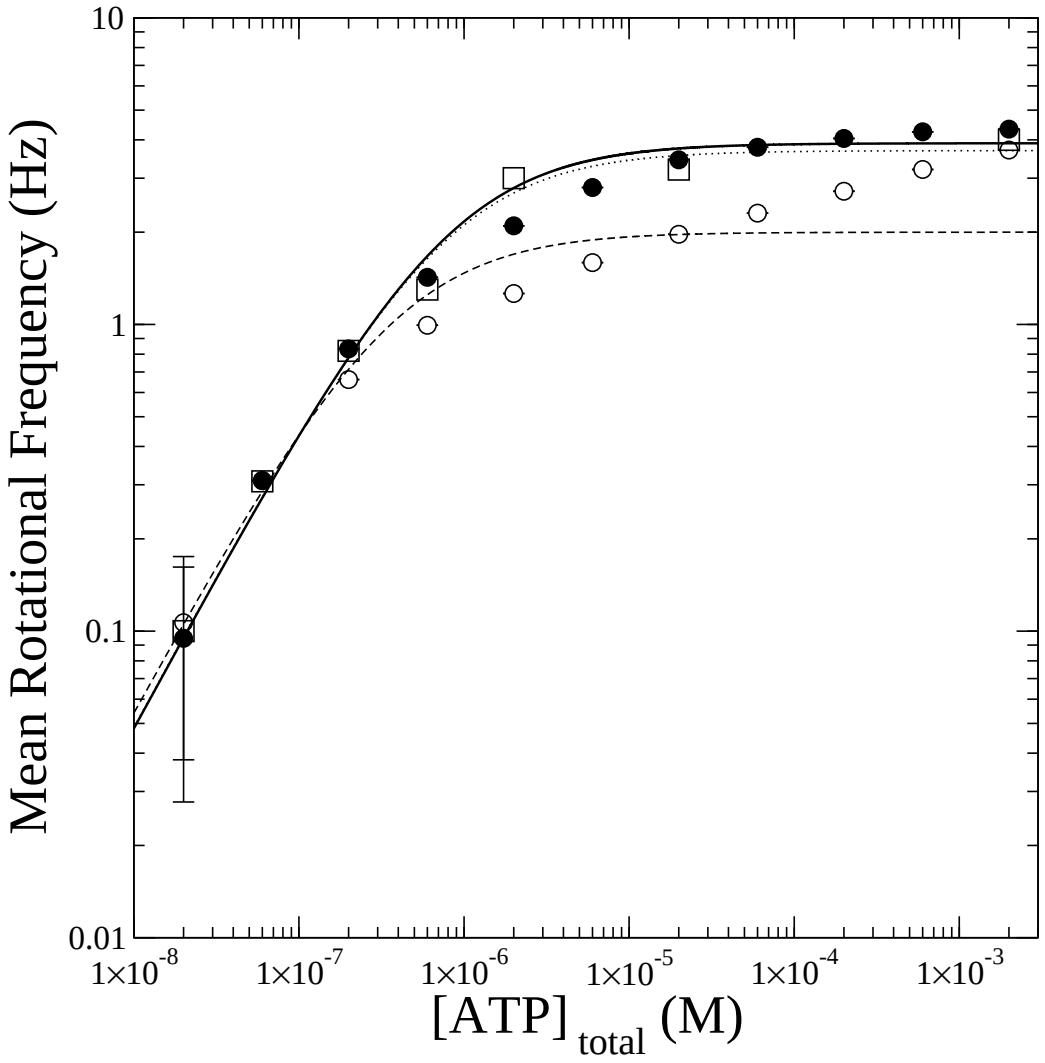
10
1
0.1
0.01
Mean Rotational Frequency (Hz)
1×10-8
1×10-7
1×10-6
1×10-5
1×10-4
1×10-3
[ATP] total (M)

Figure 9